

Emergent *c*-axis magnetic helix in manganite-nickelate superlatticesG. Fabbri,^{1,2,*} N. Jaouen,³ D. Meyers,¹ J. Feng,^{4,†} J. D. Hoffman,^{5,6,‡} R. Sutarto,⁷ S. G. Chiuabăian,^{4,3}
A. Bhattacharya,^{5,6} and M. P. M. Dean^{1,§}¹*Department of Condensed Matter Physics and Materials Science, Brookhaven National Laboratory, Upton, New York 11973, USA*²*Advanced Photon Source, Argonne National Laboratory, Argonne, Illinois 60439, USA*³*Synchrotron SOLEIL, L'Orme des Merisiers, Saint-Aubin, BP 48, 91192 Gif-sur-Yvette, France*⁴*Sorbonne Université, CNRS, Laboratoire de Chimie Physique-Matière et Rayonnement, UMR 7614, 4 place Jussieu, 75252 Paris Cedex 05, France*⁵*Materials Science Division, Argonne National Laboratory, Argonne, Illinois 60439, USA*⁶*Nanoscience and Technology Division, Argonne National Laboratory, Argonne, Illinois 60439, USA*⁷*Canadian Light Source, Saskatoon, Saskatchewan S7N 2V3, Canada*

(Received 4 June 2018; revised manuscript received 14 September 2018; published 2 November 2018)

The nature of the magnetic order in $(\text{La}_{2/3}\text{Sr}_{1/3}\text{MnO}_3)_9/(\text{LaNiO}_3)_3$ superlattices is investigated using x-ray resonant magnetic reflectometry. We observe a *c*-axis magnetic helix state in the $(\text{LaNiO}_3)_3$ layers that has not been reported in bulk nickelates, and which mediates the $\sim 130^\circ$ magnetic coupling between the ferromagnetic $(\text{La}_{2/3}\text{Sr}_{1/3}\text{MnO}_3)_9$ layers, illustrating the power of x rays for discovering the magnetic state of complex oxide interfaces. Resonant inelastic x-ray scattering and x-ray absorption spectroscopy show that Ni-O ligand hole states from bulk LaNiO_3 are mostly filled due to an interfacial electron transfer from Mn, driving the Ni orbitals closer to an atomlike $3d^8$ configuration. We discuss the constraints imposed by this electronic configuration to the microscopic origin of the observed magnetic structure. The presence of a magnetic helix in $(\text{La}_{2/3}\text{Sr}_{1/3}\text{MnO}_3)_9/(\text{LaNiO}_3)_3$ is crucial for modeling the potential spintronic functionality of this system and may be important for designing emergent magnetism in novel devices in general.

DOI: [10.1103/PhysRevB.98.180401](https://doi.org/10.1103/PhysRevB.98.180401)

Interfaces between complex oxide materials exhibit remarkably rich physics driven by the interplay of various types of charge, orbital, and spin couplings [1–3]. Particularly fascinating is their proven ability to host new types of emergent magnetic order that do not exist in either of the bulk constituents, representing a challenge to our understanding of electron correlations, as well as an opportunity for exploitation in spintronic devices [2–4]. In fact, complex magnetic phases are potentially common in transition-metal oxide superlattices given the severe effects of interfacial symmetry breaking in localized $3d$ orbitals [5–10], but scrutiny over the microscopic magnetic interactions at such interfaces is often constrained by limited direct evidence of the resulting magnetic structure. Superlattices composed of manganites and nickelates are a paradigmatic venue for efforts to discover and understand emergent interface magnetism, motivated by the complex magnetic order and phase diagram of its bulk constituents [11,12]. In fact, this system harbors fascinating phenomena, such as exchange bias and interfacial electronic reconstructions [13–27].

Recently, a highly unusual magnetic coupling between ferromagnetic manganite layers was observed in [001]-oriented $(\text{La}_{2/3}\text{Sr}_{1/3}\text{MnO}_3)_9/(\text{LaNiO}_3)_n$ [(LSMO)₉/(LNO)_{*n*}, $n = 1$ –9], in which the coupling angle between (LSMO)₉ layers varies between zero and 130° as a function of n (Fig. 1) [22], an observation that, based on conceptual arguments, was suggestive of a magnetic helix in the (LNO)_{*n*} layers. Despite the demonstrated ability of this system to be used as resistive memory devices [4], experimental evidence for how or if the noncollinear magnetism of the (LSMO)₉ layers is mediated through (LNO)_{*n*} is missing. Such a lack of information critically hampers the ability to understand the physical mechanism driving the (LSMO)₉ magnetic coupling, which consequently inhibits the design of new superlattices with optimized magnetic properties.

In this Rapid Communication, we focus on the (LSMO)₉/(LNO)₃ superlattice because it displays the largest magnetic coupling angle between the manganite layers ($\gamma \approx 130^\circ$ at 25 K [22]). We probe its magnetic and electronic structure using resonant soft x-ray techniques. The magnetic structures of both (LSMO)₉ and (LNO)₃ are studied using Mn and Ni *L*-edge x-ray resonant magnetic reflectivity (XRMR). We find that the nickelate layers contain a magnetic helix in which the Ni moments are mostly confined to the basal plane and rotate around the *c* axis. Such a magnetic structure is not present in any simple perovskite nickelate nor manganite. The XRMR ability to provide a precise description of the (LSMO)₉/(LNO)₃ magnetic ordering allows for a careful analysis of the magnetic interactions

*gfabbris@anl.gov

†Present address: CAS Key Laboratory of Magnetic Materials and Devices, Ningbo Institute of Materials Technology and Engineering, Chinese Academy of Sciences, Zhejiang 315201 Ningbo, China.

‡Present address: Department of Physics, Harvard University, Cambridge, MA 02138, USA.

§mdean@bnl.gov

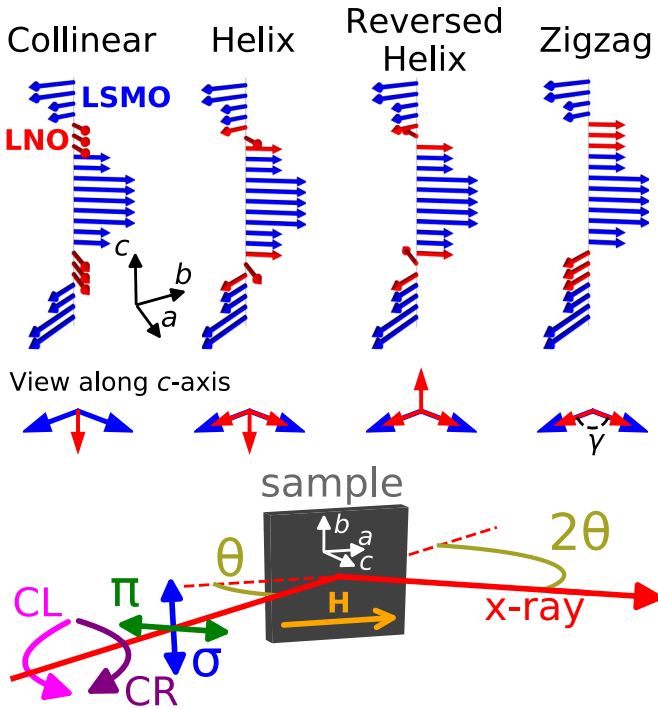


FIG. 1. Top and middle: Possible magnetic structures of the LaNiO_3 layer in $(\text{LSMO})_9/(\text{LNO})_3$. The coupling angle γ corresponds to the angle between two $(\text{LSMO})_9$ layers. Bottom: Experimental geometry used in both XRMR and RIXS measurements. XRMR was measured using circular and linear x-ray polarization with the magnetic field (H) applied along the sample's a axis. RIXS was measured using linear x-ray polarization with θ and 2θ fixed to 15° and 85° , respectively.

in this system. To this end, the nature of the Ni $3d$ and O $2p$ orbitals is probed through Ni L_3 -edge resonant inelastic x-ray scattering (RIXS) and O K -edge x-ray absorption spectroscopy (XAS) measurements. The RIXS spectra are composed of well-defined orbital excitations, which are reproduced by a model of localized Ni $3d^8$ orbitals under the effect of an octahedral crystal field. Even though the Ni $3d$ orbital is predominantly localized, O K -edge XAS shows a small Ni $3d$ -O $2p$ ligand hole concentration, indicating that the NiO_2 planes are lightly hole doped. While further work is needed to elucidate the magnetic couplings acting in this system, our analysis suggests that the $(\text{LSMO})_9/(\text{LNO})_3$ magnetic helix emerges from a combination of the strong pinning of Ni and Mn moments at the interfaces with a spin-density-wave (SDW) instability within the $(\text{LNO})_3$ layers.

High-quality $14 \times [(\text{LSMO})_9/(\text{LNO})_3]$ superlattices were grown on $[001]$ single-crystalline SrTiO_3 substrates using molecular beam epitaxy as described previously [22,28]. XRMR measurements were performed at the Ni and Mn L edges [28] at the REIXS beamline of the Canadian Light Source [35] and at the SEXTANTS beamline of the SOLEIL synchrotron [36]. Data were collected using horizontal scattering geometry, as well as both linear (σ and π) and circular [left (CL) and right (CR)] x-ray polarizations (Fig. 1). Magnetic field was applied parallel to the sample surface

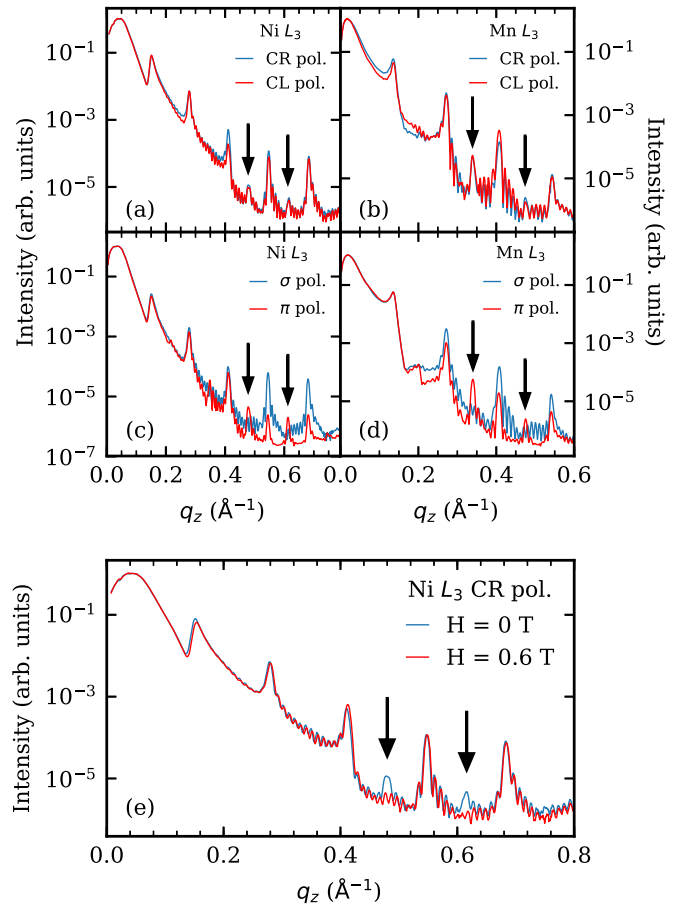


FIG. 2. (a) and (c) Ni L_3 -edge (853.6-eV) XRMR data using circular and linear polarization, respectively. (b) and (d) Mn L_3 -edge (641-eV) XRMR data using circular and linear polarization respectively. Data from both edges show half-order magnetic peaks (black arrows). This is consistent with a noncollinear magnetic structure between both LNO layers and LSMO layers as shown in Fig. 1. (e) Field dependence of the Ni L_3 XRMR data. A field of 0.6 T is sufficient to force a ferromagnetic alignment between every layer, which suppresses the half-order peaks, consistent with previous results [22].

and within the scattering plane using permanent magnets at REIXS and an electromagnet at SEXTANTS. In the former the data were collected at remanence after removing a 600-mT field, while in the latter the sample was field cooled, and measured, under 1.2 mT. The temperature was kept at ~ 25 K throughout the experiments. Data analysis was performed with the DYNAL [37] and REMAGX [38] software programs using the magnetic matrix formalism. Resonant optical constants were obtained by combining the tabulated values with averaged XAS and x-ray magnetic circular dichroism measurements [28,39].

Figure 2 displays a summary of the XRMR data collected on $(\text{LSMO})_9/(\text{LNO})_3$. The XRMR signal measured with circular light is primarily sensitive to components of the magnetization of each layer along the x-ray direction, while π polarization probes the transverse magnetization, and σ polarization is dominated by the lattice response [37,38]. It is thus clear in Figs. 2(a)–2(d) that magnetic peaks appear at

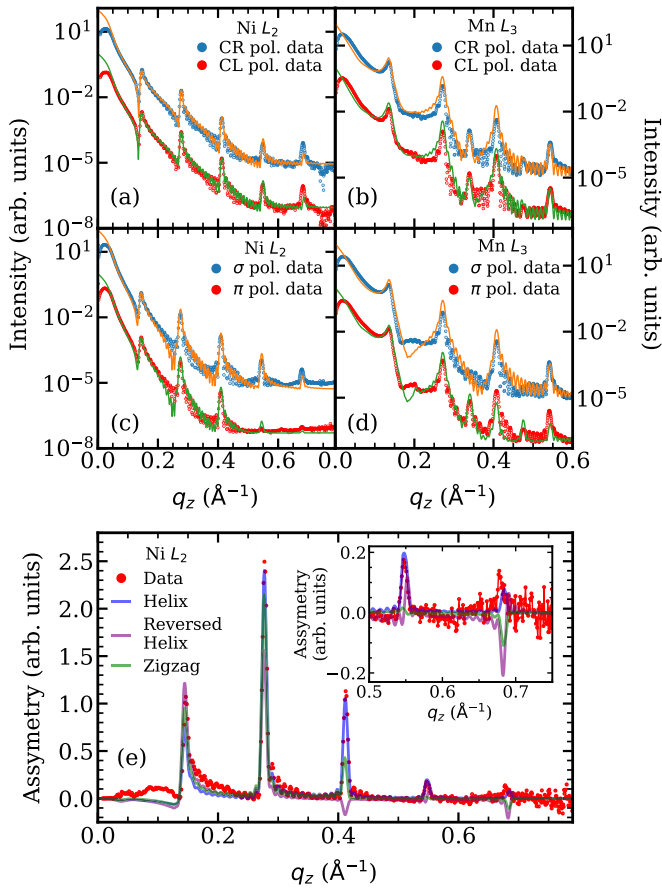


FIG. 3. Fits to the XRM signal at the Ni L_2 (871.6 eV) [(a) and (c)] and Mn L_3 [(b) and (d)] edges in $(\text{LSMO})_9/(\text{LNO})_3$. Different polarization channels CR/CL or σ/π are shown as blue/red points and are overlapped by orange/green lines representing the fit. Different channels are offset from one another for clarity. (e) displays the XRM asymmetry [42]; the helix model is consistent with the presence of peaks at high q_z .

$1/2$ order positions in $(\text{LSMO})_9/(\text{LNO})_3$ at both Mn and Ni edges, indicating that the magnetic structure unit cell along the c axis has twice the length of the chemical repetition. This observation is further demonstrated by the disappearance of such magnetic peaks when a field of 0.6 T is applied, which is sufficient to saturate the magnetic moments along the field [Fig. 2(e)] [22]. While the Mn edge results are consistent with the previous report [22], the data at the Ni edge indicate that a noncollinear magnetic structure is also present in the $(\text{LNO})_3$ layer. Additionally, the simple presence of a magnetic response in the CR/CL XRM demonstrates that there is a net magnetic moment in the NiO_2 planes [40]. Consequently, the magnetic structure of $(\text{LNO})_3$ is different from the $(\frac{1}{4} \frac{1}{4} \frac{1}{4})$ -type observed in [111]-grown LNO heterostructures and bulk RENiO_3 (RE = rare earth) as this structure would lead to a zero net moment in the NiO_2 planes [23,41]. However, this in itself does not distinguish between other $(\text{LNO})_3$ magnetic structures such as the zigzag and (reversed) helical models (Fig. 1).

The $(\text{LNO})_3$ and $(\text{LSMO})_9$ magnetic structures are determined by modeling the XRM data as shown in Fig. 3. Details of the modeling are provided in the Supplemental Material

[28]. The $(\text{LSMO})_9$ magnetic structure obtained through the Mn L_3 -edge XRM modeling is consistent with previous results [28], thus we focus here on capturing the $(\text{LNO})_3$ magnetic structure that could not be determined through neutron reflectivity [22]. Fits were performed at the Ni L_2 edge because there is a substantial overlap between the La M_4 and Ni L_3 edges, which makes the XRM data analysis very difficult. Despite its magnetic sensitivity, the XRM signal is largely dominated by charge responses [Figs. 3(a)–3(d)]. In fact, the disagreements between simulation and experimental data seen at the Mn L_3 edge are at least partially driven by the expected $\text{Mn}^{4+/3+}$ valence modulation within the $(\text{LSMO})_9$ layer [17,22,43]. We can overcome this challenge by isolating the magnetic response using the XRM circular polarization asymmetry shown in Fig. 3(e) [42]. It is clear that only the helical model is able to reproduce all features in the data, particularly at high q_z . Magnetic models with LNO spins away from the basal plane are not shown here but were also unable to reproduce the experimental data [28]. Modeling of both Mn and Ni edges is consistent with $\gamma = 140(20)^\circ$, in agreement with neutron reflectivity [22,44]. The $(\text{LNO})_3$ c -axis magnetic helix result is surprising as such structures are uncommon in bulk transition-metal oxides. This demonstrates that in $(\text{LSMO})_9/(\text{LNO})_3$ the interfacial symmetry breaking and charge transfer drive an emergent form of magnetism, the underlying electronic structure of which we now explore.

We first address the character of the nickelate layer $3d$ orbital using Ni L_3 -edge RIXS. Data were collected at 30 K using the AERHA end station of the SEXTANTS beamline at the SOLEIL synchrotron [48]. The experimental scattering geometry is detailed in Fig. 1. Figure 4 shows the RIXS spectra as a function of incident x-ray energy and linear polarization. The experimental data [Figs. 4(a) and 4(b)] are composed of narrow peaks that are consistent with dispersionless localized orbital excitations of $3d^8$ (Ni^{2+}) ions [47,49–51]; a distinctively different broad diagonal feature is seen in RIXS spectra of bulk RENiO_3 and hole-doped $\text{La}_{2-x}\text{Sr}_x\text{NiO}_4$ (for $x \geq 1/3$) [47,51,52], in which a significant amount of extra holes in the NiO_2 plane populates the hybridized Ni $3d$ -O $2p$ ligand hole states. This result is consistent with Ni L_2 -edge XAS data [22]. The RIXS spectra were simulated using the Kramers-Heisenberg equation combined with atomic multiplet calculations performed with the Cowan and RACER codes [45–47]. These simulations [Figs. 4(c) and 4(d)] nicely reproduce the observed signal [28], confirming that these are orbital dd excitations, thus demonstrating the localized character of the Ni $3d$ state in $(\text{LSMO})_9/(\text{LNO})_3$. Furthermore, the excellent agreement between experimental data and simulation implies high-spin ($S = 1$) Ni $3d^8$ orbitals under a nearly octahedral crystal field with $10D_q = 1.1$ eV and $\Delta e_g = 0.05$ eV [53].

While the RIXS results establish a predominantly localized Ni $3d$ orbital, it has minimal sensitivity to the potential presence of a small amount of Ni $3d$ -O $2p$ ligand holes. Figure 5 displays the pre-edge of the O K -edge XAS data collected in total electron yield mode at the REIXS beamline of the Canadian Light Source. The x rays were incident at 15° and the sample was field cooled to 25 K under 0.6 T, but the magnetic field was removed prior to the data collection. The pre-edge

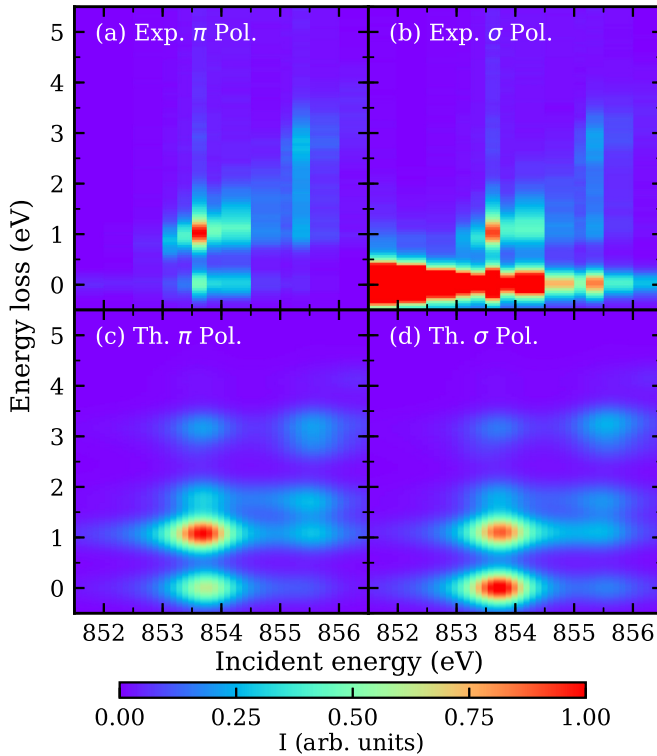


FIG. 4. Ni L_3 -edge RIXS of $(\text{LSMO})_9/(\text{LNO})_3$. Data for π and σ polarized incident x rays are displayed in (a) and (b), respectively. (c) and (d) present simulations of the RIXS spectra for π and σ polarization using atomic calculations [45–47].

is dominated by features related to Mn-O and Ni-O ligand holes. Comparing these data with the literature [54,55], it is clear that the Mn-O states dominate the signal (red box). This result is consistent with the large response expected for Mn $3d^4/3d^3$ ($\text{Mn}^{3+/4+}$) and a small or absent pre-edge structure for Ni near the $3d^8$ state (Ni^{2+}) [56–58]. It is also consistent with the position of the magnetic circular dichroism signal, which is expected to be dominated by LSMO [Figs. 5(a) and 5(c)]. However, a small pre-edge shoulder is seen at an energy that is consistent with it originating in the LNO layer (gray box). Interestingly, this feature displays a marked linear dichroism [defined here as the XAS (σ pol.)-XAS (π pol.)], implying an anisotropic ligand hole state in which more holes populate the $3d_{3z^2-r^2}2p_z$ states to the detriment of $3d_{x^2-y^2}2p_\sigma$. This result is consistent with the tensile strain applied by the SrTiO_3 substrate and is in line with the concept that strain primarily controls the Ni-O hybridization in LNO heterostructures [47,59,60].

We now discuss the consequences of the observed electronic configuration to the potential mechanisms driving the complex magnetic structure of $(\text{LSMO})_9/(\text{LNO})_3$. We start by noting that noncollinear magnetic order in transition-metal oxides may derive from the Dzyaloshinskii-Moriya interaction [61,62], but this interaction is inconsistent with the symmetry of the $(\text{LNO})_3$ magnetic structure [22]. The interfacial electronic reconstruction in $(\text{LSMO})_9/(\text{LNO})_3$ induces magnetic frustration in the nickelate layer since the antiferromagnetic Ni^{2+} -O- Ni^{2+} exchange energy is expected to be similar to the dominant ferromagnetic Ni^{2+} -O- Mn^{4+} [18,51,63,64].

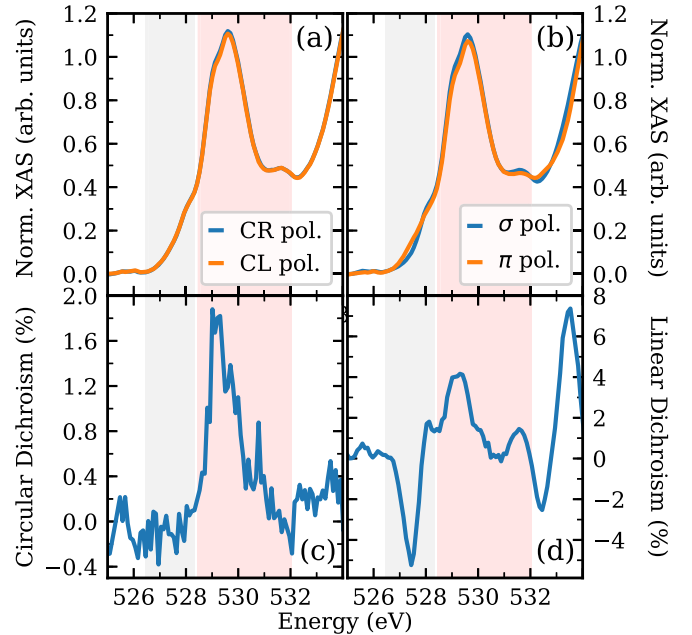


FIG. 5. $(\text{LSMO})_9/(\text{LNO})_3$ O K -edge XAS data. (a) and (b) show the pre-edge features of the XAS collected with circular and linear x rays, respectively. The circular and linear dichroisms are plotted in (c) and (d), respectively. While the signal from hybridized Mn-O orbitals dominates the pre-edge features (red box), a signal that is consistent with Ni-O hybridization is seen around 527.4 eV (gray box).

However, while we cannot exclude frustration as the sole reason for the observed spiral, if we only consider first-neighbor interactions, such frustration would arguably drive an antiferromagnetic structure that resembles the reversed helical model (see Fig. 1) since the adjacent NiO_2 planes would favor an antiferromagnetic coupling. Additionally, it is difficult to reconcile the magnetic structure LNO thickness dependence with a magnetic frustration model [22]. Emergent magnetic phenomena are often seen in systems that, much as $(\text{LSMO})_9/(\text{LNO})_3$, have $3d$ - $2p$ ligand holes (negative charge transfer systems [65]), including certain cuprates [66], hole-doped La_2NiO_4 [51,57], RENiO_3 [52], and CrO_2 [67]. In fact, it has been argued that double exchange and superexchange can act together to create noncollinear canted structures in such systems [68–70], but it is not entirely clear how such canting would actually lead to a helix. Finally, we note that the electronic structure of $(\text{LNO})_3$ closely mimics that of lightly hole-doped La_2NiO_4 [51,57,71,72], which displays stripelike spin-density-wave instabilities [73,74], which in turn are known to foster noncollinear magnetic structures [75,76]. Therefore, it appears that the $(\text{LNO})_3$ magnetic helix emerges from the coupling of such SDW instability with the interfacial Ni-Mn interaction.

In conclusion, the presence of an emergent magnetic helical structure in the $[\text{La}_{2/3}\text{Sr}_{1/3}\text{MnO}_3]_9/[\text{LaNiO}_3]_3$ superlattice is demonstrated through XRM measurements. Such a c -axis magnetic helix has not been shown to occur in other nickelate systems. Ni L_3 -edge RIXS and O K -edge XAS experiments show that interfacial charge transfer

results in NiO_2 planes with lightly hole-doped Ni $3d^8$ atoms. We argue that such an electronic structure likely drives SDW instabilities that may drive the helical magnetic structure, but further work is required to verify our arguments. Besides theoretical investigations, we believe that the role of octahedral rotations in this system needs to be addressed as these are known to be relevant to magnetic exchange. Nevertheless, the prospect of engineering spin-density waves through interfaces to create novel magnetism is tantalizing, and, in principle, such an approach should be applicable to the various families of negative charge transfer transition-metal oxides [65].

We thank Dr. Daniel Haskel for insightful discussions and Dr. Alessandro Nicolaou for support during the RIXS measurements at the SEXTANTS beamline. This material is based upon work supported by the US Department of Energy,

Office of Basic Energy Sciences, Early Career Award Program under Award No. 1047478. Work at Brookhaven National Laboratory is supported by the US Department of Energy, Office of Science, Office of Basic Energy Sciences, under Contract No. DE-SC0012704. Work at Argonne is supported by the US Department of Energy, Office of Science, under Contract No. DE-AC-02-06CH11357. Part of the research described in this Rapid Communication was performed at the Canadian Light Source, which is supported by the Canada Foundation for Innovation, Natural Sciences and Engineering Research Council of Canada, the University of Saskatchewan, the Government of Saskatchewan, Western Economic Diversification Canada, the National Research Council Canada, and the Canadian Institutes of Health Research. We acknowledge SOLEIL for provision of synchrotron radiation facilities. S.G.C. acknowledges the support of the Agence Nationale de la Recherche (ANR), under Grant No. ANR-05-NANO-074 (HR-RXRS).

-
- [1] P. Zubko, S. Gariglio, M. Gabay, P. Ghosez, and J.-M. Triscone, Interface physics in complex oxide heterostructures, *Annu. Rev. Condens. Matter Phys.* **2**, 141 (2011).
- [2] A. Bhattacharya and S. J. May, Magnetic oxide heterostructures, *Annu. Rev. Mater. Res.* **44**, 65 (2014).
- [3] F. Hellman, A. Hoffmann, Y. Tserkovnyak, G. S. D. Beach, E. E. Fullerton, C. Leighton, A. H. MacDonald, D. C. Ralph, D. A. Arena, H. A. Dürr, P. Fischer, J. Grollier, J. P. Heremans, T. Jungwirth, A. V. Kimel, B. Koopmans, I. N. Krivorotov, S. J. May, A. K. Petford-Long, J. M. Rondinelli, N. Samarth, I. K. Schuller, A. N. Slavin, M. D. Stiles, O. Tchernyshyov, A. Thiaville, and B. L. Zink, Interface-induced phenomena in magnetism, *Rev. Mod. Phys.* **89**, 025006 (2017).
- [4] J. D. Hoffman, S. M. Wu, B. J. Kirby, and A. Bhattacharya, Tunable Noncollinear Antiferromagnetic Resistive Memory through Oxide Superlattice Design, *Phys. Rev. Appl.* **9**, 044041 (2018).
- [5] S. Banerjee, O. Erten, and M. Randeria, Ferromagnetic exchange, spin-orbit coupling and spiral magnetism at the $\text{LaAlO}_3/\text{SrTiO}_3$ interface, *Nat. Phys.* **9**, 626 (2013).
- [6] X. Li, W. V. Liu, and L. Balents, Spirals and Skyrmions in Two-Dimensional Oxide Heterostructures, *Phys. Rev. Lett.* **112**, 067202 (2014).
- [7] S. Fust, S. Mukherjee, N. Paul, J. Stahn, W. Kreuzpaintner, P. Böni, and A. Paul, Realizing topological stability of magnetic helices in exchange-coupled multilayers for all-spin-based system, *Sci. Rep.* **6**, 33986 (2016).
- [8] P. Moetakef, J. R. Williams, D. G. Ouellette, A. P. Kajdos, D. Goldhaber-Gordon, S. J. Allen, and S. Stemmer, Carrier-Controlled Ferromagnetism in SrTiO_3 , *Phys. Rev. X* **2**, 021014 (2012).
- [9] A. Brinkman, M. Huijben, M. van Zalk, J. Huijben, U. Zeitler, J. C. Maan, W. G. van der Wiel, G. Rijnders, D. H. A. Blank, and H. Hilgenkamp, Magnetic effects at the interface between non-magnetic oxides, *Nat. Mater.* **6**, 493 (2007).
- [10] M. Hepting, R. J. Green, Z. Zhong, M. Bluschke, Y. E. Suyolcu, S. Macke, A. Frano, S. Catalano, M. Gibert, R. Sutarto, F. He, G. Cristiani, G. Logvenov, Y. Wang, P. A. van Aken, P. Hansmann, M. Le Tacon, J.-M. Triscone, G. A. Sawatzky, B. Keimer, and E. Benckiser, Complex magnetic order in nickelate slabs, *Nat. Phys.* (2018), doi:10.1038/s41567-018-0218-5.
- [11] C. Zener, Interaction between the d -shells in the transition metals. II. Ferromagnetic compounds of manganese with perovskite structure, *Phys. Rev.* **82**, 403 (1951).
- [12] J. B. Torrance, P. Lacorre, A. I. Nazzari, E. J. Ansaldo, and Ch. Niedermayer, Systematic study of insulator-metal transitions in perovskites $R\text{NiO}_3$ ($R = \text{Pr}, \text{Nd}, \text{Sm}, \text{Eu}$) due to closing of charge-transfer gap, *Phys. Rev. B* **45**, 8209 (1992).
- [13] K. R. Nikolaev, A. Bhattacharya, P. A. Kraus, V. A. Vas'ko, W. K. Cooley, and A. M. Goldman, Indications of antiferromagnetic interlayer coupling in $\text{La}_{2/3}\text{Ba}_{1/3}\text{MnO}_3/\text{LaNiO}_3$ multilayers, *Appl. Phys. Lett.* **75**, 118 (1999).
- [14] K. R. Nikolaev, A. Y. Dobin, I. N. Krivorotov, W. K. Cooley, A. Bhattacharya, A. L. Kobrinskii, L. I. Glazman, R. M. Wentzovitch, E. D. Dahlberg, and A. M. Goldman, Oscillatory Exchange Coupling and Positive Magnetoresistance in Epitaxial Oxide Heterostructures, *Phys. Rev. Lett.* **85**, 3728 (2000).
- [15] J. C. Rojas Sánchez, B. Nelson-Cheeseman, M. Granada, E. Arenholz, and L. B. Steren, Exchange-bias effect at $\text{La}_{0.75}\text{Sr}_{0.25}\text{MnO}_3/\text{LaNiO}_3$ interfaces, *Phys. Rev. B* **85**, 094427 (2012).
- [16] M. Gibert, P. Zubko, R. Scherwitzl, J. Íñiguez, and J.-M. Triscone, Exchange bias in LaNiO_3 - LaMnO_3 superlattices, *Nat. Mater.* **11**, 195 (2012).
- [17] J. Hoffman, I. C. Tung, B. B. Nelson-Cheeseman, M. Liu, J. W. Freeland, and A. Bhattacharya, Charge transfer and interfacial magnetism in $(\text{LaNiO}_3)_n/(\text{LaMnO}_3)_2$ superlattices, *Phys. Rev. B* **88**, 144411 (2013).
- [18] A. T. Lee and M. J. Han, Charge transfer, confinement, and ferromagnetism in $\text{LaMnO}_3/\text{LaNiO}_3$ (001) superlattices, *Phys. Rev. B* **88**, 035126 (2013).
- [19] M. Gibert, M. Viret, A. Torres-Pardo, C. Piamonteze, P. Zubko, N. Jaouen, J.-M. Tonnerre, A. Mougín, J. Fowlie, S. Catalano, A. Gloter, O. Stéphan, and J.-M. Triscone, Interfacial control of magnetic properties at $\text{LaMnO}_3/\text{LaNiO}_3$ interfaces, *Nano Lett.* **15**, 7355 (2015).

- [20] C. Piamonteze, M. Gibert, J. Heidler, J. Dreiser, S. Rusponi, H. Brune, J.-M. Triscone, F. Nolting, and U. Staub, Interfacial properties of $\text{LaMnO}_3/\text{LaNiO}_3$ superlattices grown along (001) and (111) orientations, *Phys. Rev. B* **92**, 014426 (2015).
- [21] X. Ning, Z. Wang, and Z. Zhang, Fermi level shifting, charge transfer and induced magnetic coupling at $\text{La}_{0.7}\text{Ca}_{0.3}\text{MnO}_3/\text{LaNiO}_3$ interface, *Sci. Rep.* **5**, 8460 (2015).
- [22] J. D. Hoffman, B. J. Kirby, J. Kwon, G. Fabbris, D. Meyers, J. W. Freeland, I. Martin, O. G. Heinonen, P. Steadman, H. Zhou, C. M. Schlepütz, M. P. M. Dean, S. G. E. te Velthuis, J.-M. Zuo, and A. Bhattacharya, Oscillatory Noncollinear Magnetism Induced by Interfacial Charge Transfer in Superlattices Composed of Metallic Oxides, *Phys. Rev. X* **6**, 041038 (2016).
- [23] M. Gibert, M. Viret, P. Zubko, N. Jaouen, J.-M. Tonnerre, A. Torres-Pardo, S. Catalano, A. Gloter, O. Stéphan, and J.-M. Triscone, Interlayer coupling through a dimensionality-induced magnetic state, *Nat. Commun.* **7**, 11227 (2016).
- [24] M. Kitamura, K. Horiba, M. Kobayashi, E. Sakai, M. Minohara, T. Mitsuhashi, A. Fujimori, T. Nagai, H. Fujioka, and H. Kumigashira, Spatial distribution of transferred charges across the heterointerface between perovskite transition metal oxides LaNiO_3 and LaMnO_3 , *Appl. Phys. Lett.* **108**, 111603 (2016).
- [25] J. Zang, G. Zhou, Y. Bai, Z. Quan, and X. Xu, The exchange bias of $\text{LaMnO}_3/\text{LaNiO}_3$ superlattices grown along different orientations, *Sci. Rep.* **7**, 10557 (2017).
- [26] C. L. Flint, A. Vailionis, H. Zhou, H. Jang, J.-S. Lee, and Y. Suzuki, Tuning interfacial ferromagnetism in $\text{LaNiO}_3/\text{CaMnO}_3$ superlattices by stabilizing nonequilibrium crystal symmetry, *Phys. Rev. B* **96**, 144438 (2017).
- [27] C. L. Flint, H. Jang, J.-S. Lee, A. T. N'Diaye, P. Shafer, E. Arenholz, and Y. Suzuki, Role of polar compensation in interfacial ferromagnetism of LaNiO_3 superlattices, *Phys. Rev. Materials* **1**, 024404 (2017).
- [28] See Supplemental Material at <http://link.aps.org/supplemental/10.1103/PhysRevB.98.180401> for information on the sample characterization, Mn, Ni L -edge, and O K -edge x-ray absorption spectroscopy data, as well as further details on the atomic simulation of the Ni L -edge resonant inelastic x-ray scattering data, which includes Refs. [20,22,29–34,37–39,47,51,52].
- [29] J. E. Hamann-Borrero, S. Macke, W. S. Choi, R. Sutarto, F. He, A. Radi, I. Elfimov, R. J. Green, M. W. Haverkort, V. B. Zabolotny, H. N. Lee, G. A. Sawatzky, and V. Hinkov, Valence-state reflectometry of complex oxide heterointerfaces, *npj Quantum Mater.* **1**, 16013 (2016).
- [30] J. van Elp, B. G. Searle, G. A. Sawatzky, and M. Sacchi, Ligand hole induced symmetry mixing of d^8 states in $\text{Li}_x\text{Ni}_{1-x}\text{O}$, as observed in Ni $2p$ x-ray absorption spectroscopy, *Solid State Commun.* **80**, 67 (1991).
- [31] M. Abbate, F. M. F. de Groot, J. C. Fuggle, A. Fujimori, Y. Tokura, Y. Fujishima, O. Strebel, M. Domke, G. Kaindl, J. van Elp, B. T. Thole, G. A. Sawatzky, M. Sacchi, and N. Tsuda, Soft-x-ray-absorption studies of the location of extra charges induced by substitution in controlled-valence materials, *Phys. Rev. B* **44**, 5419 (1991).
- [32] C. Aruta, G. Ghiringhelli, V. Bisogni, L. Braicovich, N. B. Brookes, A. Tebano, and G. Balestrino, Orbital occupation, atomic moments, and magnetic ordering at interfaces of magnetite thin films, *Phys. Rev. B* **80**, 014431 (2009).
- [33] P. Carra, B. T. Thole, M. Altarelli, and X. Wang, X-Ray Circular Dichroism and Local Magnetic Fields, *Phys. Rev. Lett.* **70**, 694 (1993).
- [34] H. Guo, A. Gupta, M. Varela, S. Pennycook, and J. Zhang, Local valence and magnetic characteristics of $\text{La}_2\text{NiMnO}_6$, *Phys. Rev. B* **79**, 172402 (2009).
- [35] D. G. Hawthorn, F. He, L. Venema, H. Davis, A. J. Achkar, J. Zhang, R. Sutarto, H. Wadati, A. Radi, T. Wilson, G. Wright, K. M. Shen, J. Geck, H. Zhang, V. Novák, and G. A. Sawatzky, An in-vacuum diffractometer for resonant elastic soft x-ray scattering, *Rev. Sci. Instrum.* **82**, 073104 (2011).
- [36] N. Jaouen, J.-M. Tonnerre, G. Kapoujian, P. Taunier, J.-P. Roux, D. Raoux, and F. Sirotti, An apparatus for temperature-dependent soft x-ray resonant magnetic scattering, *J. Synchrotron Radiat.* **11**, 353 (2004).
- [37] M. Elzo, E. Jal, O. Bunau, S. Grenier, Y. Joly, A. Y. Ramos, H. C. N. Tolentino, J. M. Tonnerre, and N. Jaouen, X-ray resonant magnetic reflectivity of stratified magnetic structures: Eigenwave formalism and application to a W/Fe/W trilayer, *J. Magn. Magn. Mater.* **324**, 105 (2012).
- [38] S. Macke and E. Goering, Magnetic reflectometry of heterostructures, *J. Phys.: Condens. Matter* **26**, 363201 (2014).
- [39] C. T. Chantler, Theoretical form factor, attenuation, and scattering tabulation for $Z = 1-92$ from $E = 1-10$ eV to $E = 0.4-1.0$ MeV, *J. Phys. Chem. Ref. Data* **24**, 71 (1995).
- [40] While we are unable to determine the magnetic structure within the NiO_2 planes, an x-ray magnetic circular dichroism sum rules analysis suggests a canted antiferromagnetic coupling [28].
- [41] V. Scagnoli, U. Staub, Y. Bodenthin, M. García-Fernández, A. M. Mulders, G. I. Meijer, and G. Hammerl, Induced non-collinear magnetic order of Ni^{3+} in NdNiO_3 observed by resonant soft x-ray diffraction, *Phys. Rev. B* **77**, 115138 (2008).
- [42] The XRMR asymmetry is defined here as the difference between right and left polarized XRMR times q_z^4 .
- [43] M. Zwiebler, J. E. Hamann-Borrero, M. Vafaee, P. Komissinskiy, S. Macke, R. Sutarto, F. He, B. Büchner, G. A. Sawatzky, L. Alff, and J. Geck, Electronic depth profiles with atomic layer resolution from resonant soft x-ray reflectivity, *New J. Phys.* **17**, 083046 (2015).
- [44] We estimate the uncertainty on determining the in- and out-of-plane magnetic moment angles to be $\sim 20^\circ$ and $\sim 30^\circ$, respectively [28].
- [45] R. D. Cowan, *The Theory of Atomic Structure and Spectra* (University of California Press, Berkeley, 1981).
- [46] F. de Groot and A. Kotani, *Core Level Spectroscopy of Solids* (CRC Press, Boca Raton, FL, 2008).
- [47] G. Fabbris, D. Meyers, J. Okamoto, J. Pellicciari, A. S. Disa, Y. Huang, Z. Y. Chen, W. B. Wu, C. T. Chen, S. Ismail-Beigi, C. H. Ahn, F. J. Walker, D. J. Huang, T. Schmitt, and M. P. M. Dean, Orbital Engineering in Nickelate Heterostructures Driven by Anisotropic Oxygen Hybridization Rather Than Orbital Energy Levels, *Phys. Rev. Lett.* **117**, 147401 (2016).
- [48] S. G. Chiuzbăian, C. F. Hague, A. Avila, R. Delaunay, N. Jaouen, M. Sacchi, F. Polack, M. Thomasset, B. Lagarde, A. Nicolaou, S. Brignolo, C. Baumier, J. Lüning, and J.-M. Mariot, Design and performance of AERHA, a high acceptance high resolution soft x-ray spectrometer, *Rev. Sci. Instrum.* **85**, 043108 (2014).
- [49] G. Ghiringhelli, M. Matsubara, C. Dallera, F. Fracassi, R. Gusmeroli, A. Piazzalunga, A. Tagliaferri, N. B. Brookes,

- A. Kotani, and L. Braicovich, NiO as a test case for high resolution resonant inelastic soft x-ray scattering, *J. Phys.: Condens. Matter* **17**, 5397 (2005).
- [50] G. Ghiringhelli, A. Piazzalunga, C. Dallera, T. Schmitt, V. N. Strocov, J. Schlappa, L. Patthey, X. Wang, H. Berger, and M. Grioni, Observation of Two Nondispersive Magnetic Excitations in NiO by Resonant Inelastic Soft-X-Ray Scattering, *Phys. Rev. Lett.* **102**, 027401 (2009).
- [51] G. Fabbris, D. Meyers, L. Xu, V. M. Katukuri, L. Hozoi, X. Liu, Z.-Y. Chen, J. Okamoto, T. Schmitt, A. Uldry, B. Delley, G. D. Gu, D. Prabhakaran, A. T. Boothroyd, J. van den Brink, D. J. Huang, and M. P. M. Dean, Doping Dependence of Collective Spin and Orbital Excitations in the Spin-1 Quantum Antiferromagnet $\text{La}_{2-x}\text{Sr}_x\text{NiO}_4$ Observed by X Rays, *Phys. Rev. Lett.* **118**, 156402 (2017).
- [52] V. Bisogni, S. Catalano, R. J. Green, M. Gibert, R. Scherwitzl, Y. Huang, V. N. Strocov, P. Zubko, S. Balandeh, J.-M. Triscone, G. Sawatzky, and T. Schmitt, Ground-state oxygen holes and the metal-insulator transition in the negative charge-transfer rare-earth nickelates, *Nat. Commun.* **7**, 13017 (2016).
- [53] Best agreement with the experimental data was obtained with $\Delta t_{2g} = 0$ and reduced Slater-Condon parameters: $F_{dd} = 70\%$, $F_{pd} = 85\%$, and $G_{pd} = 70\%$. We point out that the $\Delta e_g = 0.05$ eV found here implies that Δt_{2g} is likely finite. However, it also suggests a $\Delta t_{2g} < 0.01$ eV, which is smaller than our sensitivity.
- [54] J. M. Alonso, R. Cortés-Gil, L. Ruiz-González, J. M. González-Calbet, A. Hernando, M. Vallet-Regí, M. E. Dávila, and M. C. Asensio, Influence of the synthetic pathway on the properties of oxygen-deficient manganese-related perovskites, *Eur. J. Inorg. Chem.* **2007**, 3350 (2017).
- [55] B. Cui, C. Song, F. Li, G. Y. Wang, H. J. Mao, J. J. Peng, F. Zeng, and F. Pan, Tuning the entanglement between orbital reconstruction and charge transfer at a film surface, *Sci. Rep.* **4**, 4206 (2015).
- [56] P. Kuiper, D. E. Rice, D. J. Buttrey, H.-J. Lin, and C. T. Chen, Isotropic O 1s prepeak as evidence for polarons in $\text{La}_2\text{NiO}_{4+\delta}$, *Physica B* **208-209**, 271 (1995).
- [57] E. Pellegrin, J. Zaanen, H.-J. Lin, G. Meigs, C. T. Chen, G. H. Ho, H. Eisaki, and S. Uchida, O 1s near-edge x-ray absorption of $\text{La}_{2-x}\text{Sr}_x\text{NiO}_{4+\delta}$: Holes, polarons, and excitons, *Phys. Rev. B* **53**, 10667 (1996).
- [58] Y. Cao, X. Liu, M. Kareev, D. Choudhury, S. Middey, D. Meyers, J.-W. Kim, P. J. Ryan, J. W. Freeland, and J. Chakhalian, Engineered Mott ground state in a $\text{LaTiO}_{3+\delta}/\text{LaNiO}_3$ heterostructure, *Nat. Commun.* **7**, 10418 (2016).
- [59] N. Parragh, G. Sangiovanni, P. Hansmann, S. Hummel, K. Held, and A. Toschi, Effective crystal field and Fermi surface topology: A comparison of *d*- and *dp*- orbital models, *Phys. Rev. B* **88**, 195116 (2013).
- [60] M. N. Grisolia, J. Varignon, G. Sanchez-Santolino, A. Arora, S. Valencia, M. Varela, R. Abrudan, E. Weschke, E. Schierle, J. E. Rault, J.-P. Rueff, A. Barthélémy, J. Santamaria, and M. Bibes, Hybridization-controlled charge transfer and induced magnetism at correlated oxide interfaces, *Nat. Phys.* **12**, 484 (2016).
- [61] I. Dzyaloshinsky, A thermodynamic theory of “weak” ferromagnetism of antiferromagnetics, *J. Phys. Chem. Solids* **4**, 241 (1958).
- [62] T. Moriya, Anisotropic superexchange interaction and weak ferromagnetism, *Phys. Rev.* **120**, 91 (1960).
- [63] K. Nakajima, K. Yamada, S. Hosoya, T. Omata, and Y. Endoh, Spin-wave excitations in two dimensional antiferromagnet of stoichiometric La_2NiO_4 , *J. Phys. Soc. Jpn.* **62**, 4438 (1993).
- [64] D. Haskel, G. Fabbris, N. M. Souza-Neto, M. van Veenendaal, G. Shen, A. E. Smith, and M. A. Subramanian, Stability of the ferromagnetic ground state of $\text{La}_2\text{MnNiO}_6$ against large compressive stress, *Phys. Rev. B* **84**, 100403 (2011).
- [65] D. Khomskii, Unusual valence, negative charge-transfer gaps and self-doping in transition-metal compounds, [arXiv:cond-mat/0101164](https://arxiv.org/abs/cond-mat/0101164).
- [66] T. Mizokawa, H. Namatame, A. Fujimori, K. Akeyama, H. Kondoh, H. Kuroda, and N. Kosugi, Origin of the Band Gap in the Negative Charge-Transfer-Energy Compound NaCuO_2 , *Phys. Rev. Lett.* **67**, 1638 (1991).
- [67] M. A. Korotin, V. I. Anisimov, D. I. Khomskii, and G. A. Sawatzky, CrO_2 : A Self-Doped Double Exchange Ferromagnet, *Phys. Rev. Lett.* **80**, 4305 (1998).
- [68] P. G. de Gennes, Effects of double exchange in magnetic crystals, *Phys. Rev.* **118**, 141 (1960).
- [69] M. Mostovoy, Helicoidal Ordering in Iron Perovskites, *Phys. Rev. Lett.* **94**, 137205 (2005).
- [70] T. S. Santos, B. J. Kirby, S. Kumar, S. J. May, J. A. Borchers, B. B. Maranville, J. Zarestky, S. G. E. te Velthuis, J. van den Brink, and A. Bhattacharya, Delta Doping of Ferromagnetism in Antiferromagnetic Manganite Superlattices, *Phys. Rev. Lett.* **107**, 167202 (2011).
- [71] P. Kuiper, J. van Elp, D. E. Rice, D. J. Buttrey, H.-J. Lin, and C. T. Chen, Polarization-dependent nickel 2*p* x-ray-absorption spectra of $\text{La}_2\text{NiO}_{4+\delta}$, *Phys. Rev. B* **57**, 1552 (1998).
- [72] Based on comparing the Ni L_2 -edge XAS and L_3 -edge RIXS with the literature [30,31,51], we roughly estimate an average ~ 0.1 – 0.3 holes/Ni in the $(\text{LNO})_3$ layers.
- [73] J. M. Tranquada, D. J. Buttrey, V. Sachan, and J. E. Lorenzo, Simultaneous Ordering of Holes and Spins in $\text{La}_2\text{NiO}_{4.125}$, *Phys. Rev. Lett.* **73**, 1003 (1994).
- [74] V. Sachan, D. J. Buttrey, J. M. Tranquada, J. E. Lorenzo, and G. Shirane, Charge and spin ordering in $\text{La}_{2-x}\text{Sr}_x\text{NiO}_{4.00}$ with $x = 0.135$ and 0.20 , *Phys. Rev. B* **51**, 12742 (1995).
- [75] B. I. Shraiman and E. D. Siggia, Mobile Vacancies in a Quantum Heisenberg Antiferromagnet, *Phys. Rev. Lett.* **61**, 467 (1988).
- [76] O. Zachar, S. A. Kivelson, and V. J. Emery, Landau theory of stripe phases in cuprates and nickelates, *Phys. Rev. B* **57**, 1422 (1998).